Lateral diffusion in an archipelago

Dependence on tracer size

Michael J. Saxton

Institute of Theoretical Dynamics, University of California, Davis, California 95616; and Laboratory of Chemical Biodynamics, Lawrence Berkeley Laboratory, University of California, Berkeley, California 94720 USA

ABSTRACT In a pure fluid-phase lipid, the dependence of the lateral diffusion coefficient on the size of the diffusing particle may be obtained from the Saffman–Delbrück equation or the free-volume model. When diffusion is obstructed by immobile proteins or domains of gel-phase lipids, the obstacles yield an additional contribution to the size dependence. Here this contribution is examined using Monte Carlo calculations. For random point and hexagonal obstacles, the diffusion coefficient depends strongly on the size of the diffusing particle, but for fractal obstacles—cluster–cluster aggregates and multicenter diffusion-limited aggregates—the diffusion coefficient is independent of the size of the diffusing particle. The reason is that fractals have no characteristic length scale, so a tracer sees on average the same obstructions, regardless of its size. The fractal geometry of the excluded area for tracers of various sizes is examined. Percolation thresholds are evaluated for a variety of obstacles to determine how the threshold depends on tracer size and to compare the thresholds for compact and extended obstacles.

INTRODUCTION

Lateral diffusion measurements can be used as a probe of submicroscopic domain structure in lipid bilayers (1–4). In particular, recent experiments on lateral diffusion of fluorescent lipid probes have shown a percolation transition during lateral phase separation in binary lipid mixtures (1, 5–8). The concentration at which the transition occurs depends on the lipid mixture used. In one mixture, as little as 20% gel phase (by mass) was sufficient to block long-range lateral diffusion (7).

If the concentration of obstacles is below the percolation threshold, then there is a continuous path for lateral diffusion over long distances, and long-range lateral diffusion, as measured in fluorescence photobleaching recovery experiments, is allowed. Above the threshold, all long-range paths are blocked, the long-range diffusion coefficient is zero, and only short-range diffusion is possible.

The lowest percolation threshold observed by Vaz et al. (7) was 20% by mass, corresponding to an area fraction of ~16% (6), much lower than the thresholds normally encountered in the percolation literature (9). One question considered here is what obstacle geometry can yield such a low threshold. We therefore find the percolation threshold for a variety of obstacle shapes. We also examine the percolation threshold for two random fractal obstacles, cluster–cluster aggregates (CCAs) and multicenter diffusion-limited aggregates (MDLAs). Two distinct types are used to see what properties are model dependent.

In the CCA model (10, 11), particles are placed at random on a lattice at a prescribed concentration and carry out random walks, sticking irreversibly on contact. The resulting clusters also diffuse, but at a reduced rate. The process is continued until only one cluster remains.

Diffusion-limited aggregation (DLA) has been studied extensively (12, 13). There is one immobile seed particle, and one mobile particle diffuses at a time, starting far from the cluster and sticking to the cluster on contact. An extended structure is formed because the mobile particle is more likely to stick to a growing tip than to penetrate the fjords.

In the MDLA model (14), point particles are placed at random on a lattice. A few particles are randomly designated as seeds and remain immobile; the rest of the particles carry out random walks. A mobile particle binds irreversibly when it moves to a point that is adjacent to a seed particle or a previously immobilized particle. The process is continued until all the particles are immobilized. In MDLA, unlike DLA, there is more than one seed, and the mobile particles are present at nonzero concentration.

In CCA, clusters diffuse and penetrate other clusters; in DLA and MDLA, single particles diffuse and penetrate the growing cluster. In CCA, mobile particles stick to each other, but in DLA and MDLA they do not.

The other question to be considered is how the diffusion coefficient of a mobile tracer particle depends on the size of the tracer. For a pure fluid-phase lipid, the effect of the size of the diffusing particle on the lateral diffusion coefficient can be obtained from the free volume model (15) or the Saffman–Delbrück model (16) as appropriate (17). Here we examine the additional size dependence that results when diffusion is obstructed by barriers of gel-phase lipid or immobile protein. We assume that the observed diffusion coefficient can be written as

$$D = D_0(R)D^*(C, R), \qquad (1)$$

where C is the area fraction of obstacles, R is the radius of the diffusing particle, $D_0(R)$ is the diffusion coefficient for a pure fluid-phase lipid, and the entire C dependence

Address correspondence to M. J. Saxton at the Institute of Theoretical Dynamics, University of California, Davis, CA 95616.

0006-3495/93/04/1053/10 $2.00

is contained in $D^*(C, R)$, which is obtained from Monte Carlo calculations.

We use Monte Carlo calculations to show that for nonfractal obstacles—random points and random hexagons—the diffusion coefficient is strongly dependent on tracer size. For random fractal obstacles, however, the diffusion coefficient is independent of tracer size over a significant range of tracer sizes. This result is new but has a simple explanation. Fractals by definition have no characteristic length scale (reference 18, pp. 11–15). They are the same, at least statistically, on all length scales. So a tracer sees on average the same obstructions, regardless of its size, and has the same diffusion coefficient.

METHODS

CCA

The CCA calculations are carried out by standard methods (10, 11) and are described in detail elsewhere (19). A 256 × 256 triangular lattice is used, with periodic boundary conditions. Initially, particles are placed on randomly chosen sites at a prescribed concentration. Adjacent particles are assumed to form clusters, and isolated particles form clusters of unit mass. The clusters then carry out a random walk. Whenever two clusters become adjacent, they are merged irreversibly into a rigid cluster, with probability one. They move as a unit thereafter, with a translational diffusion coefficient inversely proportional to mass. The random walk continues until only one cluster remains. As long as smaller clusters move faster than larger clusters, the exact dependence of the diffusion coefficient on mass has little effect on the final structure of the aggregate (20).

MDLA

The MDLA calculations are carried out by standard methods (14). Again, a 256 × 256 triangular lattice is used, with periodic boundary conditions. Prescribed concentrations of mobile and immobile particles are placed at random on the lattice. Typically, the concentration of immobile ("seed") particles is 1/1024, and the total concentration of particles ranges between 0.025 and 0.200. The mobile particles carry out random walks. When a mobile particle becomes adjacent to a seed particle or an immobilized particle, it sticks irreversibly and becomes immobilized. The process continues until all the particles are immobilized.

Diffusion

Diffusion calculations are carried out as described earlier (19, 21). In the case of point or hexagonal obstacles, the obstacles are placed on the lattice at random. Hexagonal obstacles are not allowed to overlap, even at edges or vertices. In the case of CCA and MDLA, the aggregates are generated as previously described and their position is fixed. Then, for all the types of obstacles, a tracer is placed at a random unblocked point on the lattice and carries out a random walk on unobstructed lattice sites. The position of the tracer is recorded periodically. The calculation is repeated for various starting positions of the tracer within a given configuration of obstacles and for various configurations of obstacles at the same concentration. The mean-square displacement of the tracer is obtained as a function of time, and the diffusion coefficient D^* is calculated as described earlier (21). The diffusion coefficient is normalized to one when no obstacles are present. Typically, 25 different configurations of obstacles and 200 different tracers within each configuration of obstacles were used. In each obstacle configuration, each tracer was moved for $1–2 \times 10^6$ time steps. The statistical error is similar to that found earlier (19). For hexagonal tracers of radius 1, three independent runs at an area fraction of 0.050 yielded $D^* = 0.5122 \pm 0.0040$ for point obstacles and $D^* = 0.3440 \pm 0.0204$ for CCAs. Aggregates are less uniform than random points are, so the scatter in D^* is greater.

For diffusion of a hexagonal tracer of radius (or side) R_{EX}, the obstacles are expanded by R_{EX} lattice constants. As discussed below, diffusion of a tracer of radius R_{EX} in the presence of the original obstacles is equivalent to diffusion of a point tracer in the presence of the expanded obstacles.

Calculation of percolation thresholds

The site percolation threshold is the lowest concentration of obstacles at which there is a spanning cluster of obstacles in the infinite lattice. A spanning cluster is a cluster of obstacles that extends across the entire lattice, blocking long-range diffusion of a tracer. (In the calculations described here, the test actually used was for a spanning cluster of unobstructed points. The two criteria are equivalent.)

To find the threshold, one calculates for lattices of different widths the cumulative probability of the occurrence of a spanning cluster as a function of the area fraction of obstacles and extrapolates to an infinite lattice (22–24).

For obstacles of fixed shape, such as points or dimers, obstacles are added at random to a lattice until a spanning cluster occurs in both X and Y directions. The number of obstacles is recorded when a spanning cluster first appears in the X direction and when one first appears in the Y direction. This is repeated an appropriate number of times, the results for percolation in the X direction are pooled with those for percolation in the Y direction, and a histogram of the number of obstacles present at percolation is constructed. This histogram is then summed to give the required cumulative distribution curve. To test whether the obstacles form a spanning cluster, the cluster analysis algorithm of Hoshen and Kopelman (25) is used, without periodic boundary conditions. For a lattice size $L = 32$, 1,600 runs were carried out; for $L = 64$, 400; for $L = 128$, 100; and for $L = 256$, 25. The resolution is set by the number of obstacles added between tests for a spanning cluster and is given as a fraction of L^2. To allow for the steepening of the probability curves as L increased, the resolution was varied. Typically, a resolution of 1/128 was used for $L = 32$ and 64 and a resolution of 1/512 for $L = 128$ and 256.

For aggregates, the procedure is modified because one cannot just generate an aggregate, add a few more particles, and let the new particles diffuse and stick to the aggregate. Instead, the aggregate is generated at a given concentration and tested for the presence of a spanning cluster. This is repeated for a series of aggregates at that concentration and for a series of concentrations. From this, one obtains the fraction of aggregates yielding a spanning cluster, as a function of concentration.

The cumulative probability curves are then fit to an incomplete β function (22, 23) by a nonlinear least-squares program (reference 26, pp. 521–528). The form of the curve is

$$B(x) = \frac{\Gamma(a+b)}{\Gamma(a)\Gamma(b)} \int_0^x t^{a-1}(1-t)^{b-1}\,dt, \qquad (2)$$

where Γ is the gamma function and a and b are adjustable parameters fit by the program. This curve yields the area fraction $\langle C(L)\rangle = a/(a+b)$ at which the probability of a spanning cluster is 50% for a lattice of size L, and this value is extrapolated to infinite lattice size.

To extrapolate the results, a scaling law is used (9, 27). The probability of occurrence of a spanning cluster, $R(C, L)$, is a function of L/ξ, where ξ is the correlation length. The correlation length is related to the distance from the percolation threshold C_P by

$$\xi = (C - C_P)^{-\nu}, \qquad (3)$$

where ν is the scaling exponent for the correlation length, equal to 4/3 in two dimensions (9). So

$$L/\xi = L(C - C_P)^{\nu}, \quad (4)$$

and, neglecting higher-order corrections, the probability can be written as

$$R(C, L) = F[L^{1/\nu}(C - C_P)], \quad (5)$$

where F is an unknown function. This equation leads to two methods of finding the percolation threshold. First, when $C = C_P$, $R = F(0)$, independent of lattice size. So the curves of R versus C intersect at a point, independent of L, and that point is the percolation threshold. Second, if we take R to be constant, say 0.50, then $C = \langle C(L) \rangle$, and Eq. 5 yields

$$\langle C(L) \rangle = C_P + kL^{-1/\nu}, \quad (6)$$

where k is a constant. One can then plot $\langle C(L) \rangle$ versus $L^{-1/\nu}$ and obtain the percolation threshold C_P by linear extrapolation. This is the primary method used in this paper to evaluate the threshold. In the extrapolation, the points for L = 32, 64, 128, and 256 are weighted equally. The larger grids are inherently more accurate, because boundary effects are smaller and the curves are much steeper, but one can get better statistics with the smaller grids (1,600 grids for L = 32 versus 25 grids for L = 256). It is assumed that these two factors compensate.

Error analysis of percolation thresholds

On the basis of the detailed examination of the values for points and dimers given here, error limits of ±0.0015 are assumed for all the thresholds. We show here that for points on the triangular lattice, the Monte Carlo results agree, to within the error bars, with the exact value (9) of ½ and that various estimates of the threshold for dimers agree within the error bars.

First, consider the assumption that the cumulative probability curve can be fit by an incomplete β function. All that is used from the fit is $\langle C(L) \rangle$, the 50% point of the curve. This point was also found by fitting the center five points to a straight line. The two estimates typically agreed to three decimal places; in the few cases of major disagreement (~2% difference), the straight line was influenced by statistical noise near the center and the incomplete β function better represented the data. So the use of the incomplete β function is justified. The error from assuming a particular functional form is negligible compared with the statistical fluctuations among runs.

Second, consider the definition of a spanning cluster. One could require spanning in one direction or in both. Cumulative probability curves were obtained and the extrapolations to $L \to \infty$ carried out for spanning in either direction, spanning in both directions, and the average of the two (23, 24). The extrapolated average is taken to be the threshold, and the larger difference between the threshold and the other two extrapolated values is taken as an error estimate (24). Application of this method to the Monte Carlo data yields a threshold of 0.4995 ± 0.0011 for points and 0.4866 ± 0.0005 for dimers.

Third, consider the differences between independent runs. Three runs were done for L = 128 to give error bars for $\langle C(L) \rangle$. The same error bars were assumed for the other values of $\langle C(L) \rangle$, and the extrapolation was carried out using the extreme straight lines through the error bars. This yielded a threshold of 0.4990 ± 0.0015 for point tracers with point obstacles and 0.1156 ± 0.0014 for hexagonal tracers of unit radius with point obstacles. For dimers, three full sets of runs for L = 32–256 were carried out, giving three values of the threshold, 0.4863 ± 0.0009.

Fourth, the intersections of the curves for $R(C, L)$ for different values of L provide another estimate of the threshold. The intersections are evaluated by fitting incomplete β functions to the Monte Carlo data. These values agree well with the other estimates, though the scatter among the points of intersection is much greater. For points, the threshold is 0.4996 ± 0.0027 and for dimers, 0.4866 ± 0.0043. For all 14 geometries considered, the ratio of the threshold from extrapolation to the threshold from intersection was 0.9983 ± 0.0023, and the worst case gave a ratio of 0.9929.

The data for aggregates is noisier than the other data because there were fewer repetitions. For CCAs, there is no threshold. For MDLAs, an incomplete β function could be fit to the data despite the noise, and the thresholds from extrapolation and from intersection agreed as well as they did for the other types of obstacles.

Correlation function

The pair correlation function is obtained by Fourier transformation (reference 26, pp. 449–453) and is averaged over 100 different configurations. The statistical error is small; in similar curves for CCAs on the square lattice (19), three independent runs gave curves indistinguishable on the scale of the figure.

RESULTS

First, we consider the lateral diffusion coefficient as a function of the area fraction of obstacles and the tracer size. Then, to understand the dependence on tracer size, we consider the excluded area and, for fractal obstacles, its fractal nature. Finally, we consider the percolation threshold for various obstacles, including the threshold for the excluded area. Preliminary results were presented earlier (28, 29).

Lateral diffusion

The diffusion coefficient is found by Monte Carlo calculations. Obstacles are placed on a lattice, an inert point tracer is placed on a random unblocked site, and the tracer carries out a random walk on unobstructed sites. The mean-square displacement of the tracer is calculated as a function of time, yielding the diffusion coefficient $D^*(C)$, normalized to one at C = 0. Concentrations of obstacles are expressed as area fractions C, defined as the fraction of lattice points occupied by obstacles. The unit of length is the lattice constant l. To translate calculated quantities into observable quantities, l may be taken to be the size of a lipid or the size of a protein (19).

For nonfractal obstacles, D^* depends strongly on the size of the tracer, as shown in Fig. 1, *A* and *B*, in which the diffusion coefficient is given as a function of the area fraction of obstacles. For random point obstacles, there is a very strong dependence on tracer size. For random nonoverlapping hexagonal obstacles, there is a strong dependence on tracer size.

For fractal obstacles, however, the diffusion coefficients are almost independent of tracer size over a significant range of tracer sizes and obstacle concentrations, as shown in Fig. 1 *C*. For CCAs, there is little dependence on tracer size, except for a slight decrease at the highest concentrations. For MLDAs, there is a consistent decrease in the diffusion coefficient with tracer radius, but the decrease is small.

Fig. 1 shows that for point tracers, random points are more effective obstacles than the same area fraction of hexagonal obstacles, as shown by Eisinger et al. (30). CCAs are much more effective obstacles than the same area fraction of random point obstacles (19). For hexago-

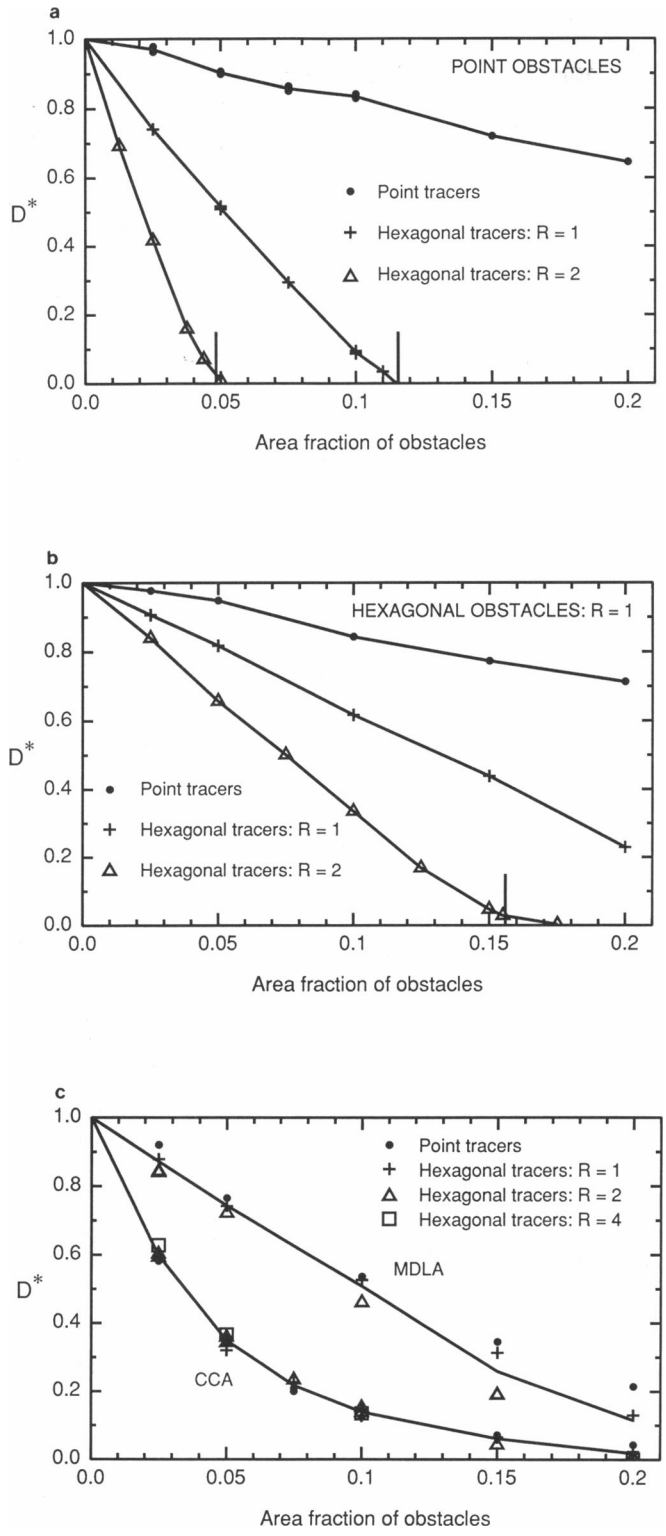

FIGURE 1 Normalized diffusion coefficient D^* as a function of the area fraction of obstacles for hexagonal tracers of radius 0, 1, 2, and 4. Vertical lines in *a* and *b* indicate percolation thresholds. Diffusion occurs above the threshold at a low rate as a result of finite-size effects; diffusion calculations are for a 256 × 256 lattice, but the thresholds are for the infinite lattice. (*a*) Random point obstacles. (*b*) Random nonoverlapping hexagonal obstacles of radius 1. (*c*) Cluster–cluster aggregates (CCA) and multicenter diffusion-limited aggregates (MDLA). The concentration of seed particles for the MDLAs was 1/1024.

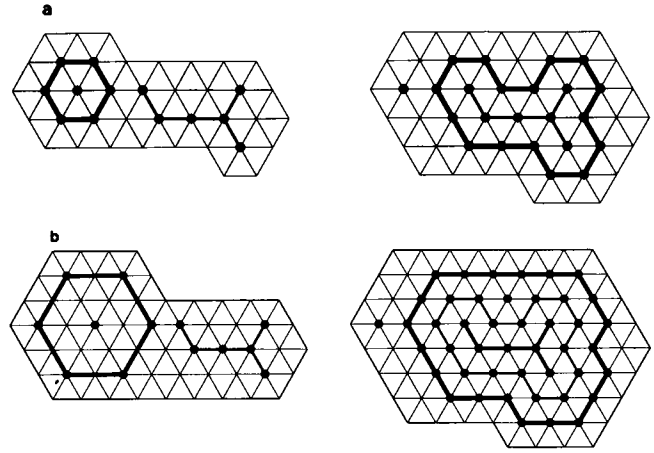

FIGURE 2 Excluded areas resulting from a cluster of point obstacles for (*a*) a hexagonal tracer of radius 1 and (*b*) a hexagonal tracer of radius 2. A hexagonal tracer of unit radius diffusing in the presence of immobile point obstacles (*left*) is equivalent to a point obstacle diffusing in the presence of enlarged obstacles (*right*). For hexagonal tracers of radius 1, the nearest neighbors of the obstacle points are blocked. For hexagonal tracers of radius 2, the next-nearest neighbors are also blocked.

nal tracers of radius 2, random point obstacles are more effective than either hexagonal obstacles or aggregates because the excluded area of random points is much greater.

Excluded area

In the random walk of a hexagonal tracer in the presence of obstacles, no point in the tracer is allowed to overlap any point of an obstacle. Equivalently, one can expand the obstacles by the radius R_{EX} of the tracer to give the excluded area for that tracer. The tracer can then be replaced by a point particle diffusing in the presence of the expanded obstacles, as done by Kim and Torquato (31), for example, in their treatment of three-dimensional diffusion. This is a useful way to visualize the effect of tracer radius. Fig. 2 shows the expansion process in detail; Fig. 3 shows large-scale examples for a tracer of radius 2 in the presence of random point obstacles, a CCA, and an MDLA.

In Fig. 3 *A*, for random point obstacles, the system is well above the percolation threshold, 0.048, for tracers of radius 2. There are few places where a tracer of radius 2 can fit, and long-range diffusion is impossible. For the fractal obstacles (Fig. 3, *B* and *C*), long-range paths for diffusion exist in both directions, and dead ends of all sizes occur in both the original obstacles and the excluded area.

In general, for the fractal obstacles in Fig. 3, all the geometric features affecting diffusion, such as fjords, bays, lakes, and straits, occur on all length scales. A point tracer sees fjords of all widths. A hexagonal tracer of radius 1 sees all but the narrowest fjords, and so forth.

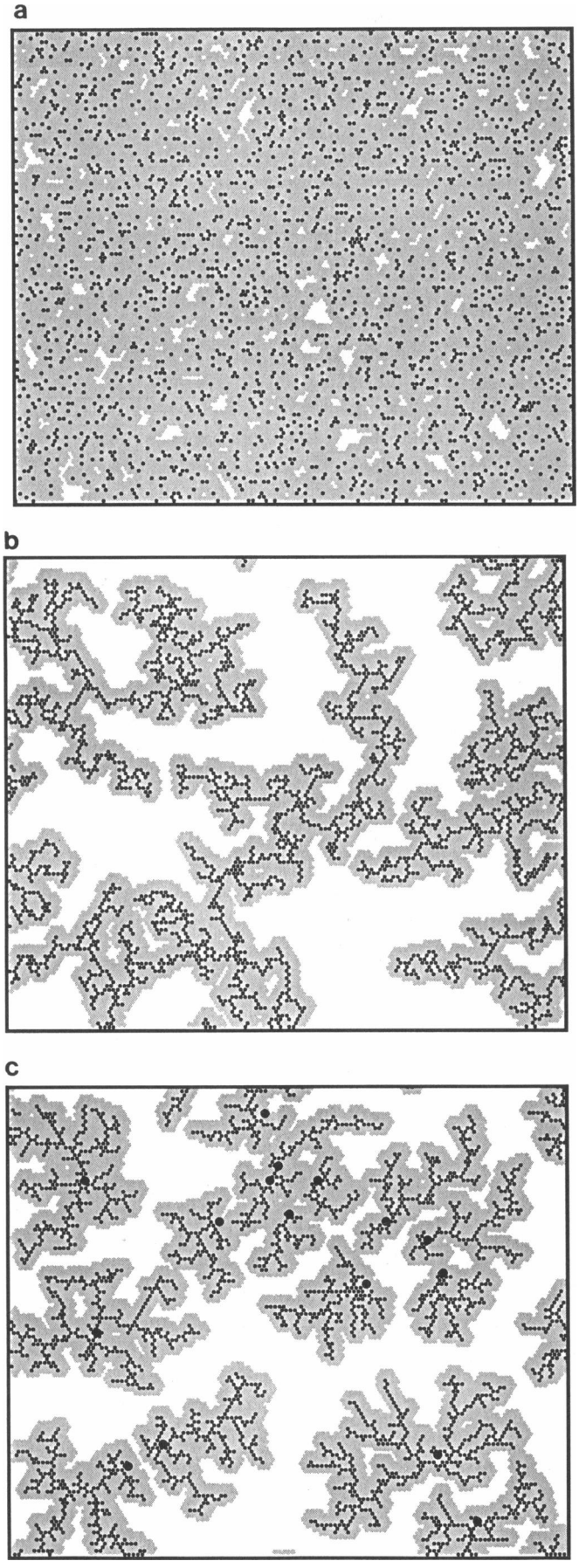

Whatever its size, a tracer sees on the average the same geometry of obstacles, and so the diffusion coefficient is independent of the size of the tracer. This argument breaks down when the tracer is so large that the finite size of the lattice affects the structure of the obstacles.

The fjords and bays are one of the reasons the fractal obstacles are so effective at blocking diffusion: they can trap diffusing particles temporarily. In a fractal obstacle, fjords and bays occur on all length scales, so trapping occurs on all time scales. The implications of this for lateral diffusion measurements are discussed by Nagle (32). The aggregates act somewhat like a gel filtration medium, trapping and delaying mobile species, but there is an essential distinction. Gel filtration media, such as Sephadex, have a characteristic length scale, though they could be fractal on smaller scales; fractals do not. Gel filtration media sort the mobile species by size; fractal obstacles do not. If a gel filtration medium were fractal over all length scales, it would be useless.

The pair correlation function

Fig. 3 suggests that the excluded area of a fractal obstacle is still fractal. To demonstrate this, we use the pair correlation function. The application of correlation functions to protein organization in membranes was reviewed by Abney and Scalettar (33).

The fractal dimension D_f is defined as follows. If M is the mass contained in a circle of radius r, then $M \sim r^{D_f}$. For an ordinary two-dimensional object, $D_f = 2$. Lower values correspond to tenuous, stringy structures. The fractal dimension of a DLA is 1.70 ± 0.06 (13). The fractal dimension of a CCA is between 1.42 and 1.75, depending on concentration (34), and the fractal dimension of a straight line is 1.

The pair correlation function $C(r)$ gives the probability that, if a particle is at $r = 0$, there is also a particle at a distance r in any cluster (19). The correlation function shows that the aggregates have a fractal structure at short distances and a uniform structure at long distances:

$$C(r) \sim \begin{cases} 1 & (r = 0) \\ r^{-(d-D_f)} & (r \ll R_{COR}) \\ C_0 & (r \gg R_{COR}), \end{cases} \qquad (7)$$

where $d = 2$ is the Euclidean dimension of the space in which aggregation occurs, D_f is the fractal dimension of the aggregate, and R_{COR} is the correlation length (20).

In Fig. 4, pair correlation functions are shown for random points, CCAs, MDLAs, and the excluded areas generated from them. For random points at an area fraction

FIGURE 3 Excluded areas for a hexagonal tracer of radius 2 in the presence of an area fraction $C = 0.15$ of obstacles: (*a*) random point obstacles; (*b*) a cluster–cluster aggregate; (*c*) a multicenter diffusion-limited aggregate with a concentration of seed particles of 1/1024. The obstacles are shown in black; the excluded area is shown in gray; and in *c* the seed particles are shown as large dots. A 128 × 128 triangular lattice is used.

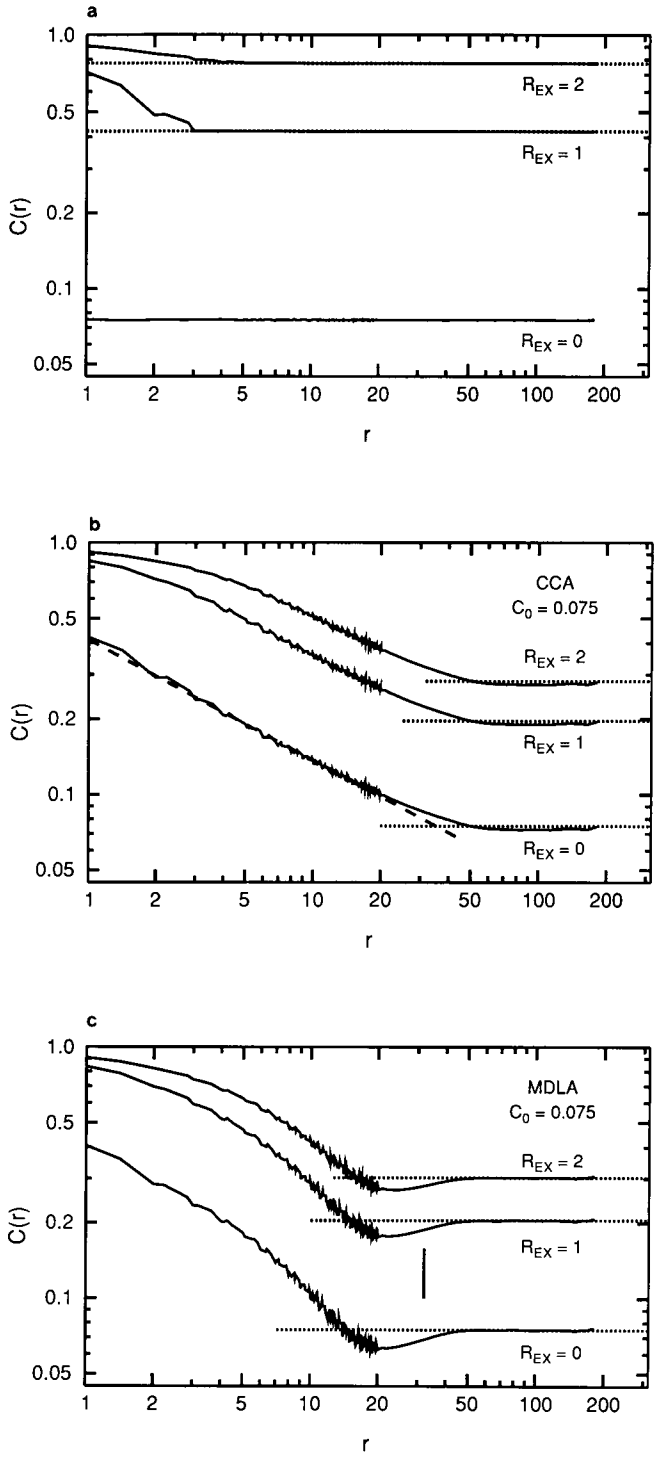

FIGURE 4 Pair correlation functions for the indicated obstacles (R_{EX} = 0) and the excluded areas generated from them (R_{EX} = 1, 2). Dotted horizontal lines represent the average concentration. The noise in the correlation functions results from the lattice structure and statistical fluctuations; the abrupt reduction in noise occurs where averages over r are plotted instead of values for individual values of r. (*a*) Random points at an area fraction of 0.075. (*b*) Cluster–cluster aggregates at an area fraction of 0.075. The dashed line represents a least-squares fit to the initial part of the curve and yields a fractal dimension D_f = 1.52. (*c*) Multicenter diffusion-limited aggregates at an area fraction of 0.075. The vertical bar indicates the average distance between seed particles for the seed concentration used (1/1024).

C_0, $C(r)$ is trivial: $C(0) = 1$ and $C(r) = C_0$ for $r > 0$, as shown in the lower curve of Fig. 4 *A*. The slope of zero corresponds to a fractal dimension of 2. The upper curves show the pair correlation function for the excluded area generated from random points. For large r, the distribution is uniform, and for small r, there is a peak, because in the excluded area all the points of the original obstacles are surrounded by obstructed points.

The pair correlation functions show the fractal structure of CCAs (19). In the lower curve in Fig. 4 *B*, there is a crossover from a straight line of slope $-(d - D_f)$ for small r to a horizontal line at large r. The aggregate is fractal over a significant length. The fractal dimension changes from 1.42 for $C_0 = 0.025$ to 1.64 for $C_0 = 0.200$. With the appropriate vertical displacements, the pair correlation functions for the excluded areas are superimposable on the curve for the original aggregate, except for flattening at small r. Again, the flattening occurs because all points of the original cluster are surrounded by obstructed points in the excluded area. The identity of the curves over much of the range of r shows that over those distances, the fractal geometry of the aggregate is the same as the fractal geometry of the excluded areas generated from it.

Unlike CCAs, MDLAs at low density are a collection of independent clusters (Fig. 3 *C*), so the pair correlation functions are different (Fig. 4 *C*). The fractal dimension for an MDLA with $C_0 = 0.200$ is 1.67. As C_0 decreases, the shape of the pair correlation function is dominated by the depletion zone between clusters. Again, the curves for R_{EX} = 0, 1, and 2 are superimposable except for flattening at small r.

Percolation thresholds

Here we find the percolation thresholds for different tracer sizes and consider how the threshold depends on the shape of the obstacle.

The thresholds are found by standard means (22–24). Obstacles are placed at random on an $L \times L$ lattice at a prescribed area fraction with no overlap permitted. The lattice is then tested for a spanning cluster of obstacles: a cluster connecting the left and right edges of the lattice or the top and bottom edges. This is repeated for various random configurations at the prescribed area fraction and for various area fractions. These calculations yield a curve for the cumulative probability that a spanning cluster is present, as a function of area fraction. In Fig. 5, cumulative probability curves for MDLAs and for equilateral triangles of three lattice points on a triangular lattice are shown for various lattice sizes. As the lattice size increases, the curves grow steeper. The points for each value of L are fit to an incomplete β function, and the midpoint of the curve is obtained. Extrapolation of the midpoints to infinite lattice size provides one value of the percolation threshold, and the point at which the curves intersect provides another. Details of the procedures are given in Methods.

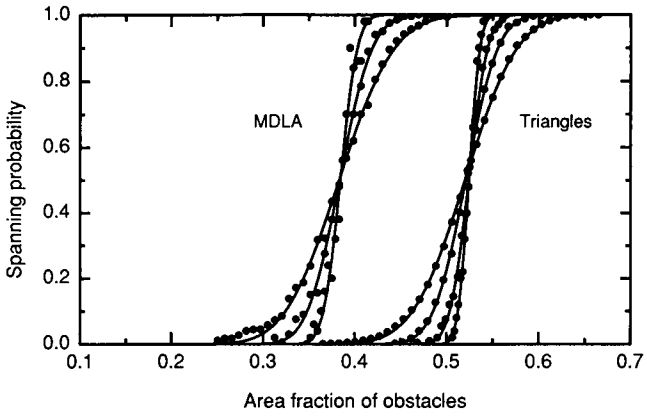

FIGURE 5 Cumulative probability that a spanning cluster of obstacles is present in either direction, as a function of the area fraction of obstacles. Data points and incomplete β functions fit to the data points are shown. The curves grow steeper as L increases. *Left*, Curves for MDLAs with lattice sizes $L = 64$, 128, and 256, and seed concentration 1/1024. *Right*, Curves for equilateral triangles of three lattice points, for lattice sizes $L = 32$, 64, 128, and 256.

To obtain the percolation threshold for tracers of nonzero radius, obstacles are placed on the lattice, and the appropriate excluded area is generated for that tracer radius. The excluded area is then tested for the presence of a spanning cluster, and the threshold found as before.

Percolation thresholds C_P for various combinations of obstacles and tracers are shown in Table 1. The thresholds are the area fraction of point obstacles needed to block diffusion of a tracer of specified radius. In the percolation literature (9), thresholds are usually given as the area fraction of conducting sites, $1 - C_P$. The error is estimated at ± 0.0015, as described in Methods. The equilateral triangle used contains 3 lattice points; a hexagon of unit radius, 7 points; and a hexagon of radius 2, 19 points. For MDLAs, the area fraction of seed particles is given in parentheses.

The percolation thresholds for tracers of various sizes reflect the sensitivity of the diffusion coefficient to tracer size shown in Fig. 1, *A* and *B*. Long-range diffusion of a point tracer is allowed if the area fraction of point obstacles is below 0.4990, diffusion of a hexagon of radius 1 is allowed if the area fraction is below 0.1156, and diffusion of a hexagonal tracer of radius 2 is allowed if the area fraction is below 0.04823. The percolation thresholds for point and hexagonal obstacles are much more sensitive to tracer size than are those for MDLAs.

As Fig. 5 shows, in a finite system above the percolation threshold, there is not always a spanning cluster of obstacles. So, even above the threshold, long-range diffusion paths can occur in a finite system, and the diffusion coefficient is nonzero, as shown in Fig. 1. For hexagonal tracers of radius 2 in the presence of hexagonal obstacles of radius 1, for example, the percolation threshold is 0.1559, but $D^* = 0.0028$ for $C = 0.1750$ on a 256×256 lattice. As the size of the system increases, the curve of spanning probability as a function of area fraction of obstacles grows steeper, as shown in Fig. 5 (See also reference 18, pp. 106–109). In the limit of an infinite system, this curve becomes a step function, and the diffusion coefficients go to zero at the percolation threshold. In an infinite system above the percolation threshold, the probability of a long-range diffusion path is vanishingly small.

Table 1 shows that compact obstacles have a higher percolation threshold than extended obstacles. The threshold for hexagons of unit radius is higher than that for points, the threshold for points is higher than that for dimers, and the threshold for dimers is higher than that for trimers. Xia and Thorpe (35) obtained an empirical formula for the percolation threshold as a function of the aspect ratio of the obstacle, based on their data for the percolation threshold of randomly centered, randomly oriented ellipses on a continuum. They found that the threshold decreases as the ellipses become more elongated. Given an observed percolation threshold, then, one can argue qualitatively that it comes from compact or extended obstacles (1, 7), although one should not take this too literally in a system of unknown and possibly complex geometry.

For MDLAs, the percolation threshold is a function of the concentration of seed particles. As the concentration of seed particles decreases, the aggregates become more extended, and the percolation threshold decreases, as Table 1 shows. One might expect a much lower threshold for a structure made up by joining fractal clusters, but, just as diffusing particles in DLA are unlikely to penetrate a fjord, in MDLA they are unlikely to reach the narrow gap between two clusters (14). See, for example, the pair of clusters in the lower left corner of Fig. 3 *C*.

For CCAs, there is no percolation threshold. Fig. 6 shows the cumulative probability curves for spanning

TABLE 1 Site percolation thresholds C_P for the triangular lattice

Tracer	Obstacle	C_P
Point	Point	0.4990
Hexagon ($R = 1$)	Point	0.1156
Hexagon ($R = 2$)	Point	0.04823
Point	Hexagon ($R = 1$)	0.5852
Hexagon ($R = 1$)	Hexagon ($R = 1$)	0.2635
Hexagon ($R = 2$)	Hexagon ($R = 1$)	0.1559
Point	MDLA (1/1,024)	0.3847
Hexagon ($R = 1$)	MDLA (1/1,024)	0.2311
Hexagon ($R = 2$)	MDLA (1/1,024)	0.1794
Point	Hexagon ($R = 1$)	0.5852
Point	Equilateral triangle	0.5256
Point	Point	0.4990
Point	Dimer	0.4863
Point	Linear trimer	0.4609
Point	MDLA (1/512)	0.4011
Point	MDLA (1/1,024)	0.3847
Point	MDLA (1/2,048)	0.3661

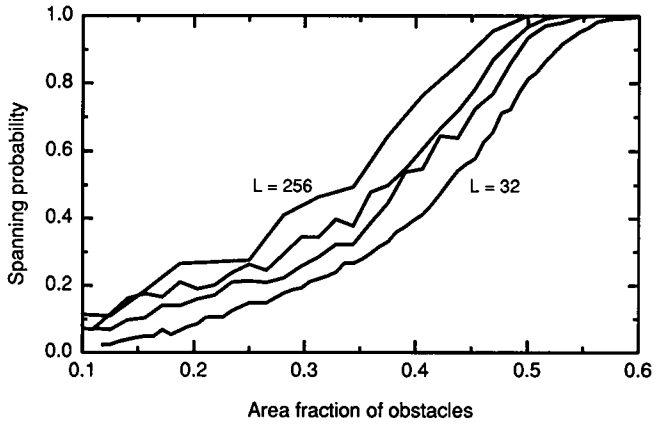

FIGURE 6 Cumulative probability that a spanning cluster is present in either direction, as a function of the area fraction of obstacles, for CCAs. Lattice sizes are L = 32, 64, 128, and 256.

clusters for CCAs. The curves do not intersect at a single point, and the intersections that occur are the result of statistical noise. The curves are parallel and do not grow steeper as the lattice size increases. As L increases, the curves show no sign of reaching a limit. The curves are asymmetrical about their midpoint and cannot be fit by an incomplete β function. The curves for CCAs are broader than those for triangles and MDLAs, and they start at a much lower concentration. For an area fraction of 0.20 and L = 128, there is a 20% probability of occurrence of a spanning cluster, able to block long-range diffusion. This curve shows one of the reasons for the effectiveness of CCAs as obstacles to lateral diffusion (19).

Why is there no percolation threshold for CCAs? If an obstacle is linear enough, then it has no percolation threshold. Consider a straight line of obstacles in an $L \times L$ lattice. To form a spanning cluster, L obstacles are needed, and the percolation threshold is $C_P = 1/L \to 0$. More generally, if a fractal of mass $M \sim r^{D_f}$ is in a d-dimensional Euclidean space, then the density is $\rho \sim M/r^d \sim 1/r^{d-D_f}$, with $d > D_f$. So the density goes to zero as $r \to \infty$, and a spanning cluster can exist at low density (36). Even though there is no percolation threshold, there still can be a spanning cluster of obstacles, able to block long-range diffusion.

Why, then, is there a percolation threshold for MDLAs? In this case there is an externally imposed length scale, the average distance between seeds. If we chose random points and constructed hexagons of prescribed radius on them, a percolation threshold would exist. MDLAs are constructed by a similar process, but instead of hexagons centered on the points, there are random fractal clusters containing the points.

DISCUSSION

The lattice model of diffusion involves several approximations, reviewed by Scalettar and Abney (37). First, continuum diffusion is replaced by lattice diffusion. This does not appear to be a major limitation. For a system of mobile particles, a continuum model of diffusion based on Brownian dynamics (37) gave diffusion coefficients in good agreement with lattice Monte Carlo results (21, 38). Second, a pure hard-core repulsive interaction between obstacles and tracers is assumed. Attractive forces and long-range repulsive forces are neglected. These may be significant (39, 40). Third, the perturbation of lipid by protein is neglected; if obstacles reduce the free volume in the surrounding lipids, then the diffusion coefficient may decrease significantly (5, 15, 41). Fourth, the model neglects hydrodynamic interactions among diffusing species, which may be significant (42). These limitations of the model are more important than the statistical error in the Monte Carlo results.

Furthermore, we have assumed that the diffusion coefficient can be written as a product of concentration-independent and concentration-dependent terms (Eq. 1). We have assumed that the obstacles are immobile on the time scale of the diffusion measurement. If they are mobile, there is no percolation threshold, and diffusion occurs at all concentrations of obstacles, at a rate that decreases with obstacle concentration (21). We have also assumed that the tracer cannot penetrate the obstacles, so the results are not applicable to the permeable protein-rich domains proposed by Yechiel and Edidin (43).

The calculations of percolation thresholds show that for point tracers the changes in threshold with obstacle shape are relatively small. For the obstacle shapes considered, all the values fall in the range of 0.35–0.60, as shown in Table 1. More extreme geometries are needed to account for the experiments of Vaz et al. (7), in which 16% gel phase (by area) was sufficient to block long-range lateral diffusion. One possibility is that the obstacles are needlelike; the percolation threshold for overlapping, randomly centered, randomly oriented ellipses becomes arbitrarily small as the ellipses become more elongated (35). Another possibility is that the actual geometry of the obstacles is more complex than the obstacles considered here, presumably a more asymmetric structure (7, 28).

The calculations of lateral diffusion coefficients lead to the main qualitative conclusion: for compact obstacles, such as random points or random hexagons, the diffusion coefficient is strongly dependent on the size of the diffusing particle but for fractal obstacles, the diffusion coefficient is practically independent of tracer size. The main quantitative results are the percolation thresholds for different tracer sizes and the corresponding curves of $D^*(C)$.

The calculations predict a large effect of tracer size on D^* for random point obstacles and hexagonal obstacles. In contrast, if all of the particles are mobile, the effect of tracer size is much less; there is a shift in D^* on going from point particles to hexagons but very little dependence on the radius of the hexagon (21). In addition, one must consider the size dependence of the diffusion

coefficient in the absence of obstacles, D_0. The R-dependence is larger in the free volume model (15, 41) than in the Saffman–Delbrück model (16).

The simplest experimental test of the calculated diffusion coefficients would be a comparison of lipid diffusion with protein diffusion or a comparison among proteins of different sizes. The problem is that the interactions with the obstacles may be different; it would be useful to compare diffusion of, say, a monomer and a multimer of the same species.

I thank P. F. F. Almeida and J. R. Abney for preprints of their papers and the reviewers for helpful comments.

This work was supported by National Institutes of Health grant GM-38133.

Received for publication 3 June 1992 and in final form 23 November 1992.

REFERENCES

1. Bultmann, T., W. L. C. Vaz, E. C. C. Melo, R. B. Sisk, and T. E. Thompson. 1991. Fluid-phase connectivity and translational diffusion in a eutectic, two-component, two-phase phosphatidylcholine bilayer. *Biochemistry.* 30:5573–5579.
2. Edidin, M., and I. Stroynowski. 1991. Differences between the lateral organization of conventional and inositol phospholipid-anchored membrane proteins. A further definition of micrometer-scale membrane domains. *J. Cell. Biol.* 112:1143–1150.
3. Ghosh, R., and W. W. Webb. 1990. Evidence for intra-membrane constraints to cell surface LDL receptor motion. *Biophys. J.* 57:286*a*. (Abstr.)
4. Lee, G. M., A. Ishihara, and K. A. Jacobson. 1991. Direct observation of Brownian motion of lipids in a membrane. *Proc. Natl. Acad. Sci. USA.* 88:6274–6278.
5. Almeida, P. F. F., W. L. C. Vaz, and T. E. Thompson. 1992. Lateral diffusion and percolation in two-phase, two-component lipid bilayers. Topology of the solid-phase domains in-plane and across the lipid bilayer. *Biochemistry.* 31:7198–7210.
6. Vaz, W. L. C. 1992. Translational diffusion in phase-separated lipid bilayer membranes. *Comments Mol. Cell. Biophys.* 8:17–36.
7. Vaz, W. L. C., E. C. C. Melo, and T. E. Thompson. 1989. Translational diffusion and fluid domain connectivity in a two-component, two-phase phospholipid bilayer. *Biophys. J.* 56:869–876.
8. Vaz, W. L. C., E. C. C. Melo, and T. E. Thompson. 1990. Fluid phase connectivity in an isomorphous, two-component, two-phase phosphatidylcholine bilayer. *Biophys. J.* 58:273–275.
9. Stauffer, D. 1985. Introduction to Percolation Theory. Taylor and Francis, London and Philadelphia. 124 pp.
10. Kolb, M., R. Botet, and R. Jullien. 1983. Scaling of kinetically growing clusters. *Phys. Rev. Lett.* 51:1123–1126.
11. Meakin, P. 1983. Formation of fractal clusters and networks by irreversible diffusion-limited aggregation. *Phys. Rev. Lett.* 51:1119–1122.
12. Meakin, P. 1988. The growth of fractal aggregates and their fractal measures. *In* Phase Transitions and Critical Phenomena. Vol. 12. C. Domb and J. L. Lebowitz, editors. Academic Press, London. 335–489.
13. Vicsek, T. 1989. Fractal Growth Phenomena. World Scientific, Singapore. 355 pp.
14. Witten, T. A., Jr., and P. Meakin. 1983. Diffusion-limited aggregation at multiple growth sites. *Phys. Rev. B* 28:5632–5642.
15. Minton, A. P. 1989. Lateral diffusion of membrane proteins in protein-rich membranes. *Biophys. J.* 55:805–808.
16. Saffman, P. G., and M. Delbrück. 1975. Brownian motion in biological membranes. *Proc. Natl. Acad. Sci. USA.* 72:3111–3113.
17. Clegg, R. M., and W. L. C. Vaz. 1985. Translational diffusion of proteins and lipids in artificial lipid bilayer membranes. A comparison of experiment with theory. *In* Progress in Protein–Lipid Interactions. Vol. 1. A. Watts and J. J. H. H. M. De Pont, editors. Elsevier, Amsterdam. 173–229.
18. Feder, J. 1988. Fractals. Plenum Press, New York. 283 pp.
19. Saxton, M. J. 1992. Lateral diffusion and aggregation: a Monte Carlo study. *Biophys. J.* 61:119–128.
20. Meakin, P. 1984. Diffusion-controlled aggregation on two-dimensional square lattices: results from a new cluster-cluster aggregation model. *Phys. Rev. B* 29:2930–2942.
21. Saxton, M. J. 1987. Lateral diffusion in an archipelago: the effect of mobile obstacles. *Biophys. J.* 52:989–997.
22. Nolte, D. D., and L. J. Pyrak-Nolte. 1991. Stratified continuum percolation: scaling geometry of hierarchical cascades. *Phys. Rev. A* 44:6320–6333.
23. Reynolds, P. J., H. E. Stanley, and W. Klein. 1980. Large-cell Monte Carlo renormalization group for percolation. *Phys. Rev. B* 21:1223–1245.
24. Yonezawa, F., S. Sakamoto, and M. Hori. 1989. Percolation in two-dimensional lattices. I. A technique for the estimation of thresholds. *Phys. Rev. B* 40:636–649.
25. Hoshen, J., and R. Kopelman. 1976. Percolation and cluster distribution. I. Cluster multiple labeling technique and critical concentration algorithm. *Phys. Rev. B* 14:3438–3445.
26. Press, W. H., B. P. Flannery, S. A. Teukolsky, and W. T. Vetterling. 1986. Numerical Recipes: The Art of Scientific Computing. Cambridge University Press, Cambridge. 818 pp.
27. Lironis, G., D. W. Heermann, and K. Binder. 1990. Finite-size scaling study of non-equilibrium percolation. *J. Phys. A* 23:L329–L334.
28. Saxton, M. J. 1991. Lateral diffusion in an archipelago: shifts in the percolation threshold. *Biophys. J.* 59:627*a*. (Abstr.)
29. Saxton, M. J. 1992. Lateral diffusion in an archipelago: effect of tracer size. *Biophys. J.* 61:504*a*. (Abstr.)
30. Eisinger, J., J. Flores, and W. P. Petersen. 1986. A milling crowd model for local and long-range obstructed lateral diffusion. *Biophys. J.* 49:987–1001.
31. Kim, I. C., and S. Torquato. 1992. Diffusion of finite-sized Brownian particles in porous media. *J. Chem. Phys.* 96:1498–1503.
32. Nagle, J. F. 1992. Long-tail kinetics in biophysics? *Biophys. J.* 63:366–370.
33. Abney, J. R., and B. A. Scalettar. 1992. Molecular crowding and protein organization in biological membranes. *In* Thermodynamics of Membrane Receptors and Channels. M. B. Jackson, editor. CRC Press, Boca Raton, FL. In press.
34. Kolb, M., and H. J. Herrmann. 1985. The sol-gel transition modelled by irreversible aggregation of clusters. *J. Phys. A* 18:L435–L441.
35. Xia, W., and M. F. Thorpe. 1988. Percolation properties of random ellipses. *Phys. Rev. A* 38:2650–2656.
36. Smirnov, B. M. 1990. The properties of fractal clusters. *Phys. Reports.* 188:1–78.
37. Scalettar, B. A., and J. R. Abney. 1991. Molecular crowding and protein diffusion in biological membranes. *Comments Mol. Cell. Biophys.* 7:79–107.
38. Pink, D. A. 1985. Protein lateral movement in lipid bilayers. Simulation studies of its dependence upon protein concentration. *Biochim. Biophys. Acta.* 818:200–204.

39. Donaldson, P. J. 1989. Modulation of lateral diffusion on lipid bilayer membranes. Ph.D. thesis. Cornell University, Ithaca, NY. 196 pp.

40. Pink, D. A., D. J. Laidlaw, and D. M. Chisholm. 1986. Protein lateral movement in lipid bilayers. Monte Carlo simulation studies of its dependence upon attractive protein-protein interactions. *Biochim. Biophys. Acta.* 863:9–17.

41. O'Leary, T. J. 1987. Lateral diffusion of lipids in complex biological membranes. *Proc. Natl. Acad. Sci. USA.* 84:429–433.

42. Bussell, S. J., D. L. Koch, and D. A. Hammer. 1992. Hydrodynamic interactions between proteins in biological membranes. *Biophys. J.* 61:291*a*. (Abstr.)

43. Yechiel, E., and M. Edidin. 1987. Micrometer-scale domains in fibroblast plasma membranes. *J. Cell Biol.* 105:755–760.